3. A SUCCESSIVE LINEAR ESTIMATOR FOR ELECTRICAL RESISTIVITY TOMOGRAPHY

Tian-Chyi J. Yeh, Junfeng Zhu, Andreas Englert, Amado Guzman, and Steve Flaherty

3.1. Introduction

A dc resistivity survey is an inexpensive and widely used technique for investigation of near surface resistivity anomalies. It recently has become popular for the investigation of subsurface pollution problems (NRC, 2000). In principle, it measures the electric potential field generated by a transmission of dc electric current between electrodes implanted at the ground surface. Then, an apparent (bulk or effective) electrical resistivity for a particular set of measurement electrodes is calculated using formulas that assume homogeneous earth. Many pairs of current transmission and electric potential measurements are used to "map" subsurface electrical resistivity anomalies.

This conventional resistivity survey is analogous to classical aquifer test in which an aquifer is excited by pumping at one well and the response of the aquifer (e.g. drawdown-time relation or well hydrograph) is observed at another well. The theoretical well hydrograph from an analytical solution that assumes aquifer homogeneity and infinite domain (e.g. Theis' solution, 1935) is then used to match the observed hydrograph to obtain apparent or effective aquifer transmissivity and storage coefficient. Due to the homogeneity assumption, the theoretical drawdown represents a spatially averaged drawdown in a heterogeneous aquifer. This average drawdown is unequivocally different from the one observed at a well in a heterogeneous aquifer, although the difference may be small due to diffusive nature of the flow process. Thus, applying Theis' solution to aquifer tests in a heterogeneous aquifer is tantamount to comparing apples to oranges (Wu et al., 2005). They suggested that the apparent transmissivity represents a weighted average of transmissivity anomalies over the cone of depression. High weights are given to transmissivity anomalies near the observation and the pumping well. The apparent transmissivity reflects, as a consequence, local geology but it can also be affected by significant geologic anomalies within the cone of depression. In other words, the physical meaning of the apparent transmissivity can be highly dubious.

The strong similarity between traditional aquifer and apparent resistivity analysis leads us to conclude that conventional analysis of electrical resistivity

H. Vereecken et al. (eds.), Applied Hydrogeophysics, 45–74.

survey is another example of comparison between apples and oranges. In fact, the apparent resistivity approach has been found virtually ineffective for environmental applications, where electrical resistivity anomalies are subtle, complex, and multi-scale (Yeh et al., 2002).

Meanwhile, a contemporary electrical resistivity survey (electrical resistivity tomography, ERT) has been designed to collect extensive electric current and electric potential data sets in multi-dimensions. The resistivity field is estimated from the inversion of the data set using, a mathematical computer model based on a regularized optimization approach and without the assumption of subsurface homogeneity (e.g. Daily et al., 1992; Ellis and Oldenburg, 1994; Li and Oldenburg, 1994; and Zhang et al., 1995). However, the general uniqueness and resolution of the three-dimensional electrical resistivity inversion have not been investigated sufficiently thus far (NRC, 2000).

While the physical process is different between electric current and groundwater flow, the governing equation for electric current and potential field created by an electrical resistivity survey is similar to that for steady flow in saturated porous media induced by pumping or injection. The mathematical inversion of an electrical resistivity survey is thus analogous to that of a groundwater aquifer test. Groundwater hydrologists and reservoir engineers have attempted to solve the inverse problem of flow through multidimensional, heterogeneous porous media for the last few decades (e.g. Gavalas et al., 1976). Reviews of the inverse problem of subsurface hydrology and various solution techniques can be found in Yeh (1986), Sun (1994), and McLaughlin and Townley (1996). The general consensus is that prior information on geological structure, and some point measurements of parameters to be estimated are necessary to better constrain solution of the inverse problem. A similar finding was also reported by Oldenburg and Li (1999) and Li and Oldenburg (2000) for the inverse problems in geophysics.

A multi-variate linear estimator (cokriging) has been widely used by groundwater hydrologists to estimate the hydraulic conductivity field from scattered measurements of pressure head and hydraulic conductivity in aquifers (e.g. Kitanidis and Vomvoris, 1983; Hoeksema and Kitanidis, 1984; Yeh and Zhang, 1996). The popularity of cokriging is attributed to its ability to incorporate spatial statistics, point measurements of hydraulic conductivity and hydraulic head into the estimation, and its ability to yield conditional mean estimates. Cokriging is also known for its ability to quantify the uncertainty associated with its estimate due to limited information and heterogeneity. Kitanidis (1997) discussed the differences between cokriging and classical inverse methods in subsurface hydrology and showed cokriging is a Bayesian formalism. Nevertheless, cokriging is a linear estimator and it is limited to mildly nonlinear systems, such as aquifers of mild heterogeneity, where the variance of the natural logarithm of hydraulic conductivity, $\sigma^2_{\ln K}$, is less than

0.1. When the degree of aquifer heterogeneity is large ($\sigma^2_{\ln K} > 1$), the linear assumption becomes inadequate and cokriging cannot take full advantage of the hydraulic head information (Yeh et al., 1996).

To overcome this shortcoming, Yeh et al. (1995, 1996), Gutjahr et al. (1994), and Zhang and Yeh (1997) developed an iterative geostatistical technique, referred to as a successive linear estimator (SLE). This technique uses a linear estimator successively to incorporate the nonlinear relation between hydraulic properties and the hydraulic head in inverse modeling. It also successively updates conditional covariances to quantify reductions in uncertainty due to successive improvements of the estimate. Yeh et al. (1995 and 1996), and Zhang and Yeh (1997) demonstrated that using the same amount of information, SLE revealed a more detailed hydraulic conductivity field than cokriging. Hughson and Yeh (2000) successfully applied SLE to the inverse problem in three-dimensional, variably saturated, heterogeneous porous media.

Based on the SLE algorithm, Yeh and Liu (2000) developed a sequential successive linear estimator (SSLE) to process the large amount of data sets created by steady-state hydraulic tomography for imaging aquifer heterogeneity. In addition, they investigated effects of monitoring intervals, pumping intervals, and the number of pumping locations on the final estimate of hydraulic conductivity. Subsequently, guidelines for design of hydraulic tomography tests were established, which are also applicable to ERT. The SSLE algorithm for hydraulic tomography was subsequently validated by Liu et al. (2002) using sandbox experiments. Robustness of SSLE compelled Zhu and Yeh (2005) to develop three-dimensional (3-D) transient hydraulic tomography, which can be used to image 3-D hydraulic conductivity and the specific storage fields in heterogeneous aquifers.

Successes of SSLE for hydraulic tomography have motivated its application to ERT. In particular, Yeh et al. (2002) developed a SSLE algorithm for ERT and investigated the effectiveness of surface and downhole electrode arrays in stratified geological media. They concluded that surface electrode arrays detect only anomalies near the surface and downhole arrays provide more accurate mapping of the anomalies at great depths. More importantly, using field core samples Baker (2001) and Yeh et al. (2002) investigated the spatial variability of Archie's law that relates moisture content to electrical resistivity. Significant spatial variability of the parameters of the law was found in a 20 m $\times$ 20 m $\times$ 15 m vadose zone in an alluvium deposit. Thereafter, numerical experiments were undertaken to demonstrate effects of the variability on ERT estimation of moisture content in the vadose zone. Finally, they cautioned interpretation of ERT for mapping changes in moisture content in the vadose zone if the variability of Archie's parameter is ignored.

To resolve the variability problem, Liu and Yeh (2004) developed an integrative ERT inversion approach based on SSLE. This integrative approach allows inclusion of prior knowledge of spatial statistics of the parameters of Archie's law and the resistivity field to be estimated as well as direct measurements of the parameters, resistivity, and moisture content values. They demonstrated how the new approach can be used to determine moisture content distribution directly without using time-lapse ERT surveys.

Since SSLE, a geostatistically based inverse model, is relatively new in geophysics, the aim of this chapter is to introduce the SSLE algorithm for ERT and to demonstrate its usefulness. Specifically, we first discuss in Section 3.2 the basic concept of stochastic representation of ERT inverse problems and then explain why the analysis of ERT survey should be viewed as a conditional mean estimation of a spatially stochastic resistivity field. In Section 3.3, the mathematical formulation of SSLE for ERT inversion is presented. Next, numerical examples are used to illustrate the robustness of the algorithm and the concept of ERT (namely, an intelligent data collection scheme to resolve the ill-poseness of electrical resistivity inversion problem) in Section 3.4. Examples of applications of ERT to monitoring solute distributions in aquifers and moisture content distributions in the vadose zone then follow. Using these examples, we show effects on the quality of ERT inversion by conditioning with direct measurements of concentration and moisture content. Lastly, the application of the SSLE algorithm to an ERT survey in a mine leaching field is presented (Section 3.5), where a stochastic approach for eliminating biased and noisy ERT data – an important step in ERT analysis – is presented.

3.2. Stochastic Conceptualization of ERT Inverse Problems

Assume that in a geological formation, the electric current flow induced by an electrical resistivity survey can be described by

$$\nabla \cdot [\xi(\mathbf{x}) \nabla \phi(\mathbf{x})] + I(\mathbf{x}) = 0 \tag{1}$$

where $\mathbf{x}$ is the location vector (x, y, z), ϕ is the electric potential [V], $I(\mathbf{x})$ represents the electric current source per volume [A/m^3], and ξ is the electrical conductivity [S/m] within a previously defined volume, a reciprocal of the electrical resistivity, ρ[ohm-m], which is assumed to be locally isotropic. The boundary conditions associated with Equation (1) are

$$\phi|_{G_1} = \phi^* \quad \text{and} \quad \xi(x) \nabla \phi \cdot \mathbf{n}|_{G_2} = q \tag{2}$$

where ϕ^* is the electric potential specified at boundary G_1, q denotes the

prescribed electric current per unit area (current density), and $\mathbf{n}$ is the unit vector normal to the boundary G_2.

The electrical conductivity or resistivity of geologic media varies spatially due to inherent heterogeneous geologic processes (Sharma, 1997). One way to describe the spatial variability of electrical conductivity is the stochastic representation approach, similar to that used in geohydrology for the variability of hydraulic properties of aquifers and vadose zones (see Gelhar, 1993; Yeh, 1992, 1998). Specifically, the electrical conductivity field of a geologic formation is considered as a stochastic process, $\xi(\mathbf{x}, \pi)$, where π is the ensemble index, ranging from one to infinity. That is, the value of $\xi(\mathbf{x})$ at each location $\mathbf{x}$ in the formation is a random variable regardless if the value is known or unknown. The electrical conductivity field of the formation, therefore, is visualized as a collection of an infinite number of random variables in space. This stochastic process can be described by a mean, $\langle \xi(\mathbf{x}) \rangle = \Omega$ (where $\langle\ \rangle$ denotes the expected value, i.e., ensemble average or the average over the infinite number of possible realizations or π in ensemble space) and perturbations around the mean, $\omega(\mathbf{x}, \pi)$, characterized by a joint probability distribution. For simplicity, the ensemble index, π, will be dropped hereafter.

Assuming that the perturbation is a second-order stationary stochastic process (that is, the stochastic process has a stationary mean and variance as well as its covariance depends on the separation distance only), its joint probability distribution can thus be adequately represented by its mean and covariance function, $\mathbf{R}_{\omega\omega}(\boldsymbol{\eta})$, where $\boldsymbol{\eta}$ is the separation vector between electrical conductivity values at two locations. The covariance function represents in a statistical sense the spatial correlation structure (pattern) of the electrical conductivity of a geologic formation. More specifically, the spatial correlation structure states the likelihood of occurrence of the same electrical conductivity value at two different locations. Because of this stochastic representation of the electrical conductivity, the electric potential field induced during an electrical resistivity survey can also be considered as a stochastic process. It can be described by $\phi(\mathbf{x}) = V(\mathbf{x}) + v(\mathbf{x})$, where $V(\mathbf{x}) = \langle \phi(\mathbf{x}) \rangle$ and $v(\mathbf{x})$ is the perturbation of the electric potential.

Suppose that electrical conductivity measurements (referred to as the primary variable or primary information), ξ_i^* (where $i = 1, \ldots, n$, and n is the total number of electrical conductivity measurements) are available from borehole electrical resistivity surveys. From these measurements, we have estimated the mean and covariance function of the electrical conductivity field of the geologic formation. Now, suppose that an ERT survey is then conducted. For each transmission of electric current during the survey, we have collected k electric potential values, v_j^*, where $j = n + 1, n + 2, \ldots, n + k$. Hereafter, the electric potential measurements are referred to as secondary information. Now, our goal is to exploit the primary and secondary information available

to estimate the electrical conductivity distribution over the volume of the geologic formation. Mathematically, we are seeking an inverse model that can produce the electric potential and electrical conductivity fields that satisfy the following conditions. That is, they must preserve the observed electric potential and electrical conductivity values at sample locations and also satisfy underlying physical processes (i.e., the governing electric potential equation). In a conditional probability context, such electric potential field and electrical conductivity field are conditional realizations of $\phi(\mathbf{x})$ and $\xi(\mathbf{x})$ fields, respectively, among many possible realizations of the ensemble. In other words, they are a subset of the ensemble of each field, which meets the prescribed conditions.

These conditional realization of the electrical conductivity field can also be expressed as the sum of the conditional mean electrical conductivity field and its conditional perturbation field, i.e., $\xi_c(\mathbf{x}) = \Omega_c(\mathbf{x}) + \omega_c(\mathbf{x})$. The subscript c denotes the state of being conditioned. Similarly, the conditional electric potential fields can be written as $\phi_c(\mathbf{x}) = V_c(\mathbf{x}) + v_c(\mathbf{x})$. It should be noticed that as more independent data or constrains are used to condition the stochastic processes, the processes should approach particular realizations of the processes (i.e., the reality). Transmission of electric current at different locations and recording of electric potentials using the same sampling network (i.e., a tomographic survey) as in an ERT survey is tantamount to creating many independent constraints to condition the stochastic processes. Nevertheless, many possible realizations of such conditional $\xi(\mathbf{x})$ and $\phi(\mathbf{x})$ fields remain in spite of the tomographic survey. The means of these conditional fields (i.e., conditional means of $\Omega_c(\mathbf{x})$ and $V_c(\mathbf{x})$) on the other hand are unique, although not necessarily reflective of the true fields.

One way to obtain these conditional mean fields is to solve the inverse problem for all possible conditional realizations of the electrical resistivity field. An average of all of the possible realizations then yields the conditional mean electrical resistivity field (see Hanna and Yeh, 1998 and others for geohydrology applications). An alternative approach is to solve the inverse problem in terms of the conditional mean equation, as described below.

In order to formulate the conditional mean equation, we first substitute the conditional stochastic variables into the governing electric potential Equation (1) and then take the expected value of the resultant equation. The conditional-mean equation thus takes the following form

$$\nabla \cdot [\Omega_c(\mathbf{x}) \nabla V_c(\mathbf{x})] + \nabla \cdot \langle \omega_c(\mathbf{x}) \nabla v_c(\mathbf{x}) \rangle + I(\mathbf{x}) = 0 \qquad (3)$$

In Equation (3), the current source, $I(\mathbf{x})$, is treated as a deterministic constant that is known. According to Equation (3), the true conditional mean $\Omega_c(\mathbf{x})$ and $V_c(\mathbf{x})$ fields do not satisfy the continuity Equation (3) unless the second term involving the product of perturbations is zero. This term represents the

uncertainty due to a lack of information of the two variables at locations where measurements are not available. The uncertainty will vanish under two conditions, namely: 1) all the electrical conductivity values in the domain (i.e., the geologic formation) are specified exactly (i.e., $\omega_c(\mathbf{x}) = 0$); or 2) all the electric potential values in the domain are known perfectly (i.e., $v_c(\mathbf{x}) = 0$) as are the electric fluxes at the boundaries. In practice, these two conditions will never be met and evaluation of this term is intractable at this moment. Consequently, in the subsequent analysis we will assume this term is proportional to the conditional mean electric potential gradient such that we can rewrite the mean equation as

$$\nabla \cdot [\Omega_{ceff}(\mathbf{x}) \nabla V_c(\mathbf{x})] + I(\mathbf{x}) = 0 \tag{4}$$

This conditional mean equation has the same form as Equation (1) but variables are expressed as the conditional effective electrical conductivity, $\Omega_{ceff}(\mathbf{x})$, and conditional mean electric potential field, $V_c(\mathbf{x})$. The conditional effective electrical conductivity thus is a parameter field that combines the conditional mean electrical conductivity, $\Omega_c(\mathbf{x})$, and $\langle \omega_c(\mathbf{x}) \nabla v_c(\mathbf{x}) \rangle (\nabla V_c(\mathbf{x}))^{-1}$. According to this concept, the conditional effective electrical conductivity field will agree with the electrical conductivity measurements at sample locations. It yields a conditional mean electric potential field that preserves values of electric potential measurements when it is employed in the forward model, Equation (4), subject to the prescribed boundary conditions. Following this concept, an optimal inverse solution to Equation (4) seeks the conditional effective electrical conductivity field. The sequential successive linear estimator (SSLE) approach to be introduced below is designed for this purpose.

3.3. Sequential Successive Linear Estimator for ERT

Suppose that a geologic medium to be investigated is discretized into M elements and each element has an electrical conductivity value, $\xi(\mathbf{x})$. For mathematical convenience, the natural logarithm of the electrical conductivity, $\ln \xi(\mathbf{x})$, instead of $\xi(\mathbf{x})$, will be used as the stochastic process for our analysis. That is, $\ln \xi(\mathbf{x}) = F + f(\mathbf{x})$ and $\langle \ln \xi(\mathbf{x}) \rangle = F$, which is assumed to be spatially invariant (although it is not necessary). One of the advantages of using $\ln \xi(\mathbf{x})$ is that this approach avoids negative value of estimated $\xi(\mathbf{x})$ values during the inverse procedure.

To derive the conditional effective electrical conductivity that will produce a conditional mean potential field in Equation (4), SSLE starts with the classical cokriging technique to construct a cokriged, mean-removed log conductivity field. The technique uses observed electrical conductivity perturbations,

f_i^*, and the observed electric potential perturbations, v_j^*, caused by one transmission of electric current during the tomography. That is,

$$\hat{f}(\mathbf{x}_0) = \sum_{i=1}^{n} \lambda_{i0} f^*(\mathbf{x}_i) + \sum_{j=n+1}^{n+k} \mu_{j0} v^*(\mathbf{x}_j) \tag{5}$$

where $\hat{f}(\mathbf{x}_0)$ is the cokriged f value at location, $\mathbf{x}_0$. Then, we define $\hat{Y}_k(\mathbf{x}_0) = [F + \hat{f}(\mathbf{x}_0)]$ and the cokriged electrical conductivity, $\hat{\xi}_k(\mathbf{x}_0)$, is given as $\exp[\hat{Y}_k(\mathbf{x}_0)]$. The cokriging weights, λ_{i0} and μ_{j0}, in Equation (5) represent influences of observations, $f^*(\mathbf{x}_i)$ and $v^*(\mathbf{x}_j)$, at locations $\mathbf{x}_i$ and $\mathbf{x}_j$ on the estimate $\hat{f}(\mathbf{x}_0)$ at $\mathbf{x}_0$. They are evaluated from solving the following system of equations

$$\begin{aligned}
&\sum_{i=1}^{n} \lambda_{io} R_{ff}(\mathbf{x}_\ell, \mathbf{x}_i) + \sum_{j=n+1}^{n+k} \mu_{jo} R_{fv}(\mathbf{x}_\ell, \mathbf{x}_j) = R_{ff}(\mathbf{x}_0, \mathbf{x}_\ell) \qquad \ell = 1, 2, \ldots, n \\
&\sum_{i=1}^{n} \lambda_{io} R_{vf}(\mathbf{x}_\ell, \mathbf{x}_i) + \sum_{j=n+1}^{n+k} \mu_{jo} R_{vv}(\mathbf{x}_\ell, \mathbf{x}_j) = R_{vf}(\mathbf{x}_0, \mathbf{x}_\ell) \qquad \ell = n+1, \ldots, n+k
\end{aligned} \tag{6}$$

where R_{ff}, R_{vv}, and R_{fv}, are the covariance between f's and that between v's, and the cross-covariance between f's and v's, respectively. Equations (5) and (6) are applied to every location, $\mathbf{x}$, in the solution domain to estimate the $f(\mathbf{x})$ field and in turn, the $\xi(\mathbf{x})$ field. The weights in equation, in essence, ensure the estimate fields obey the statistical correlation relations of f's and v's as well as the spatial cross correlation between f's and v's. In theory, the covariance, R_{vv}, and the cross-covariance, R_{fv}, in Equation (6) can be estimated from field data sets. But good estimates require a large number of measurements. As a consequence, they are derived from a first-order numerical approximation (to be discussed later: see Equations (9)–(11)) that involves the governing equation (Equation 1) for the electric potential field induced by the ERT survey. Therefore, the cokriging estimation procedure implicitly considers the physical process of propagation of electric currents.

As mentioned in the introduction, the information of electric potential measurements is not fully utilized by cokriging because the relation between f's and v's is nonlinear while it is assumed to be linear in cokriging. To resolve this problem, a successive linear estimator is used. That is,

$$\hat{Y}_c^{(r+1)}(\mathbf{x}_0) = \hat{Y}_c^{(r)}(\mathbf{x}_0) + \sum_{j=n+1}^{n+k} \beta_{j0}^{(r)} \left[\phi^*(\mathbf{x}_j) - \phi^{(r)}(\mathbf{x}_j)\right] \tag{7}$$

where $\hat{Y}_c^{(r)}(\mathbf{x}_0)$ is the estimate of the conditional mean of $\ln \xi(\mathbf{x}_0)$ at iteration r, which is the iteration index. The estimate is equal to the cokriged log conductivity field, $\hat{Y}_k$, at $r = 0$. The residual about the mean estimate at

iteration r is defined as $y^{(r)}(\mathbf{x}_0) = \ln \xi(\mathbf{x}_0) - \hat{Y}_c^{(r)}(\mathbf{x}_0)$. In Equation (7), the terms within the bracket on the right-hand side of the equation denotes the difference between $\phi^{(r)}(\mathbf{x}_j)$, the simulated electric potential at $\mathbf{x}_j$ (i.e., the solution to Equation (4)) at iteration r, and $\phi^*(\mathbf{x}_j)$, the observed potential at the same location. The weighting coefficients, $\beta_{j0}^{(r)}$'s, similar to the cokriging weights, represent the influence of the differences between simulated and observed electric potentials at location, $\mathbf{x}_j$, to the improvement of the electrical conductivity estimate at $\mathbf{x}_0$. To ensure the improved estimate obeys the spatial correlation structure, the values of $\beta_{0j}^{(r)}$'s are determined by solving the following system of equations:

$$\sum_{j=n+1}^{n+k} \beta_{j0}^{(r)} \Lambda_{vv}^{(r)}(\mathbf{x}_\ell, \mathbf{x}_j) + \theta \delta_{j\ell} = \Lambda_{vy}^{(r)}(\mathbf{x}_0, \mathbf{x}_\ell) \text{ and } \ell = n+1, \ldots, n+k \quad (8)$$

where $\Lambda_{vv}^{(r)}$ and $\Lambda_{vy}^{(r)}$, are the residual covariance (or conditional covariance function) of v_c and cross-covariance (or conditional cross-covariance) at iteration r between v_c and y_c, respectively. In Equation (8), θ is used as a stabilizing factor and $\delta_{\ell j}$ is a Kronecker delta. Specifically, during an iteration, the stabilizing factor is added to the diagonal terms of the covariance on the left-hand side of Equation (8) to numerically condition the system of equations. This makes the matrix of the equations diagonally dominant and thus assures stability and convergence of the solution. A larger term can result in a slower convergence rate, and a smaller θ value tends to expedite the convergence but often lead to numerical instability. During each iteration, the product of a constant weighting factor of user's choice and the maximum value of the diagonal terms of $\Lambda_{vv}^{(r)}$ is assigned to be this stabilizing term. Since the maximum value of the diagonal terms of $\Lambda_{vv}^{(r)}$ changes during each iteration, the θ value changes accordingly.

The solution to Equations (6) and (8) requires knowledge of the covariance of the electric potential and its cross covariance with the electrical conductivity. We approximate them by a first-order analysis. The first-order analysis (e.g. Dettinger and Wilson, 1981) expands the electric potential at location $\mathbf{x}_i$ at the rth iteration as a first-order Taylor series:

$$\phi(\mathbf{x}_i) = \hat{V}_c^{(r)}(\mathbf{x}_i) + v_c^{(r)}(\mathbf{x}_i) \approx \mathrm{G}(\mathbf{x}_i) + \frac{\partial \mathrm{G}(\mathbf{x}_i)}{\partial \ln \xi(\mathbf{x}_j^{-1})} y^{(r)}(\mathbf{x}_j) \quad (9)$$

where G is a mathematical function that represents Equation (1) and associated boundary conditions. $\mathrm{G}(\mathbf{x}_i)$, therefore, represents $\hat{V}_c^{(r)}$at location $\mathbf{x}_i$, which is evaluated using the conductivity field, $\hat{Y}_c^{(r)}(\mathbf{x})$. The term $\frac{\partial \mathrm{G}(\mathbf{x}_i)}{\partial \ln \xi(\mathbf{x}_j)}$ denotes the sensitivity of $\hat{V}_c^{(r)}$ at location $\mathbf{x}_i$ to change of $\ln \xi$ at location $\mathbf{x}_j$. The Einstein convention is adopted in Equation (9): the repeated subscript implies

summation over its entire range. The first-order approximation of the residual $v^{(r)}(\mathbf{x}_i)$ can then be written as

$$v^{r}(\mathbf{x}_i) = \frac{\partial \mathrm{G}(\mathbf{x}_i)}{\partial \ln \xi(\mathbf{x}_j)} y^{(r)}(\mathbf{x}_j) = \mathbf{J}^{(r)} \mathbf{y}^{(r)} \tag{10}$$

where $\mathbf{J}^{(r)}$, the sensitivity matrix, can be evaluated using many different methods. We here choose the adjoint state sensitivity method (Sykes et al., 1985; Sun and Yeh, 1992; Li and Yeh, 1998; Yeh et al., 2002; Liu and Yeh, 2004) for its computational efficiency.

Using Equation (10), we then derive the approximate covariance of $v^{(r)}$ and the cross-covariance between $y^{(r)}$ and $v^{(r)}$. That is,

$$\begin{aligned} \mathbf{\Lambda}_{vv}^{(r)} &= \mathbf{J}^{(r)} \mathbf{\Lambda}_{yy}^{(r)} \mathbf{J}^{\mathrm{T}^{(r)}} \\ \mathbf{\Lambda}_{vy}^{(r)} &= \mathbf{J}^{(r)} \mathbf{\Lambda}_{yy}^{(r)} \end{aligned} \tag{11}$$

where $\mathbf{J}$ is the sensitivity matrix ($k \times M$), and superscript T stands for the transpose. $\mathbf{\Lambda}_{yy}$ is the covariance matrix of y, in which each component is given by

$$\Lambda_{yy}^{(1)}(\mathbf{x}_0, \mathbf{x}_l) = R_{ff}(\mathbf{x}_0, \mathbf{x}_\ell) - \sum_{i=1}^{n_f} \lambda_{io}\, R_{ff}(\mathbf{x}_o, \mathbf{x}_\ell) - \sum_{j=n+1}^{n+k} \mu_{jo}\, R_{fv}(\mathbf{x}_j, \mathbf{x}_\ell) \tag{12}$$

at iteration $r = 0$, where $\ell = 1, 2, \ldots, M$, and λ and μ are the cokriging coefficients. Equation (12) is the cokriging variance if $\mathbf{x}_0 = \mathbf{x}_k$, a measure of the uncertainty associated with the cokriging estimate at location $\mathbf{x}_0$. For $r \geq 1$, the covariance is evaluated according to

$$\Lambda_{yy}^{(r+1)}(\mathbf{x}_0, \mathbf{x}_\ell) = \Lambda_{yy}^{(r)}(\mathbf{x}_0, \mathbf{x}_\ell) - \sum_{i=n+1}^{n+k} \beta_{io}^{(r)}\, \Lambda_{yv}^{(r)}(\mathbf{x}_i, \mathbf{x}_\ell) \tag{13}$$

Notice that these covariances are merely approximate conditional covariances because of its first order nature. The accuracy of this approximation was investigated by Hanna and Yeh (1998).

Upon completing updating the $\hat{Y}_{\mathrm{c}}^{(r)}(\mathbf{x})$ field, the mean electric flow equation is solved again with the newly estimated $\hat{Y}_{\mathrm{c}}^{(r+1)}(\mathbf{x})$ field for a new electric potential field, $\phi(\mathbf{x})$. Then, the change of σ_f^2 (the variance of the estimated electrical conductivity field) and the change of the largest misfit in the electric potential among all the monitoring locations between two successive iterations are evaluated. If both changes are smaller than some prescribed tolerances, the iteration stops. Otherwise, new $\mathbf{\Lambda}_{vy}$ and $\mathbf{\Lambda}_{vv}$ are evaluated using Equation (11) and Equation (8) is solved again to obtain a new set of weights. The new weights are subsequently used in Equation (7) in conjunction with $\phi^*(\mathbf{x}_j) - \phi^{(r)}(\mathbf{x}_j)$ to obtain a new estimate of $\hat{Y}_{\mathrm{c}}^{(r+1)}(\mathbf{x})$.

The above discussion describes the SLE for only one set of primary and secondary information during one electric current transmission. Of course, this algorithm can simultaneously include all of the electric potential measurements collected during all the electric current transmissions during ERT. Nevertheless, the system of Equations in (6) and (8) can become extremely large and ill conditioned, and stable solutions to the equations can become difficult to obtain (Hughson and Yeh, 2000).

To avoid this problem, the electric potential data sets are analyzed sequentially. Specifically, SSLE starts the iterative process with the available electrical conductivity measurements and the electric potential data set collected from one of the electric current transmissions. Once the estimated field converges to the given criteria, the newly estimated electrical conductivity field is the effective electrical conductivity conditioned on the electric potential data due to the current transmission at the first location, and the residual electrical conductivity covariance is the corresponding conditional electrical conductivity covariance.

Subsequently, the conditional effective electrical conductivity is used to evaluate the conditional mean electric potential and sensitivity matrix, associated with the electric current transmission at the next location. Based on Equation (11), the sensitivity matrix in conjunction with the conditional electrical conductivity covariance then yields the electric potential covariance and the cross-covariance of the electric potential and the electrical conductivity fields that correspond to the current transmission at this new location. These covariance and cross-covariance are subsequently employed in (8) to derive the new weights. With the conditional mean electric potential, new weights, and the observed electric potential, Equation (7) yields the electrical conductivity estimate, representing the estimate at the first iteration based on the information from the electric current injection at this new location as well as the previous transmission. The iterative process then proceeds to include the nonlinear relation between electric potential and electrical conductivity.

The same procedure is repeated for the next electric current transmission until all of the transmissions are considered. In essence, our sequential approach uses the estimated electrical conductivity field and its covariance, conditioned on previous sets of electric potential measurements, as prior information for the next estimation based on a new set of ERT survey data. It continues until all the data sets are fully utilized. A flow chart of the SSLE algorithm is illustrated in Figure 1. Such a sequential approach allows accumulation of high-density secondary information obtained from the electrical resistivity tomography, while maintaining the covariance matrix at a manageable size that can be solved with the least numerical difficulties. Vargas-Guzman and Yeh (1999 and 2002) provided a theoretical proof to show that such a sequential approach is identical to the simultaneous approach for linear systems. For

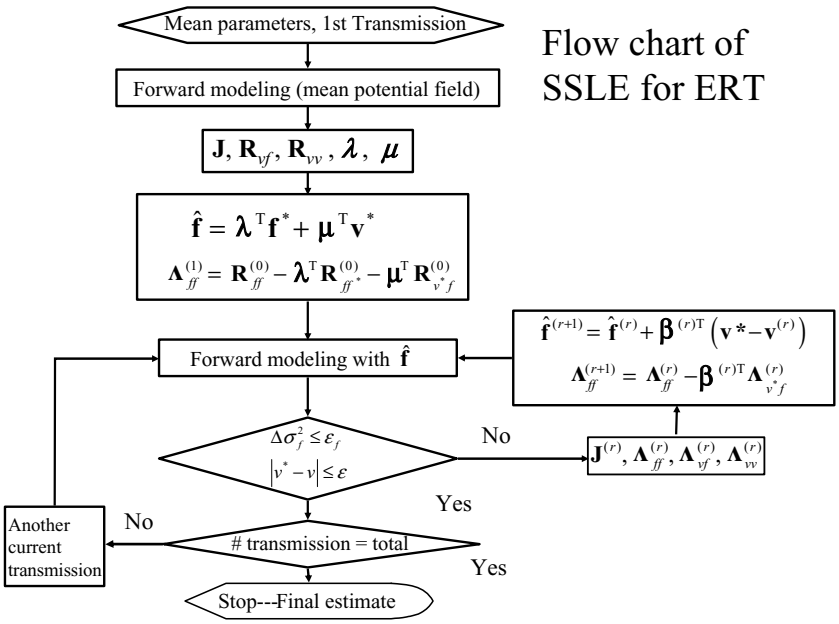

Figure 1. Flow chart showing the algorithm of SSLE for ERT

nonlinear problem as ERT, analysis of the data set in different sequence can lead to different estimates. If a large number of data are used, however, the difference is small. To avoid, this problem, the final estimate can be fed back to the SSLE algorithm to ensure a global consistency (Zhu and Yeh, 2005).

The approach is different from classical regularized optimization (Tikhonov and Arsenin, 1977) approaches that have been widely used in many engineering fields. The regularization approach seeks the smoothest parameter estimate using a somewhat "arbitrary" Tiknonov factor, ignoring our prior knowledge of the spatial structure of the parameter field. On the other hand, SSLE seeks a smooth estimate of the primary variable field that is conditioned on the spatial statistical structure representing our prior knowledge of the field.

Specifically, with a prescribed spatial mean and covariance function of the primary variable field, SSLE uses 3-D partial differential equations that govern the physics of electric flow to approximate spatial first and second moments of the secondary variable. The spatial auto-correlation of the primary and the secondary variable and their cross-correlation are subsequently derived. With measured primary and secondary variables at sample locations and the approximate auto-correlation and the cross-correlation, a linear estimator is then used to derive the estimate at any location in space – the best linear

unbiased estimates. Because of the nonlinear relation between the primary and secondary variables, the linear estimation is carried out iteratively to maximize the effectiveness of available secondary information. As a result, the estimated secondary variable satisfies the governing partial differential equations; and both estimated primary and secondary variables agree with the data (measured voltage, current, and resistivity values if any) at sampling locations. Whereas at locations where no measurements are available, the estimates are merely the approximate conditional means for the given measurements. Therefore, it is expected that SSLE will yield less smooth and more realistic estimates than the regularization approach. SSLE is a Bayesian formalism and is conceptually the same as but methodologically different from the maximum a posterior (McLaughlin and Townley, 1996) and the quasi-linear geostatistical inverse approach (Kitanidis, 1995). Lastly, we want to point out that SSLE is not limited to stationary processes; only the uncertainty estimate will be affected (i.e., less accurate) by this assumption.

3.4. Numerical Examples

In this section, we use three numerical examples to illustrate the robustness of ERT and our SSLE approach. The first example demonstrates the concept of tomographic survey under two different scenarios: a) a homogeneous resistivity field with a rectangular anomalous resistivity inclusion; b) a rectangular anomaly embedded in a randomly distributed resistivity field. The second example illustrates effects of conditioning using point measurements on ERT inversion. The last example demonstrates an integrative approach using SSLE (Liu and Yeh, 2004) and ERT to directly estimate a moisture content distribution in a 3-D heterogeneous vadose zone, where the constitutive relation between the moisture content and resistivity is spatially random.

3.4.1. EXAMPLE 1

The size of the domain examined in this example was 0.29 m in the x direction (horizontal) by 0.21 m in y direction (vertical). The domain was discretized into 609 elements with a uniform element size of 0.01 m $\times$ 0.01 m. All the boundaries were assigned as Neumann (no flow) types except at the location (0.15 m, 0.0 m) where a constant voltage of zero was assigned. The two scenarios were investigated: a) a rectangular-shape anomaly with a low electrical conductivity of 3.4000E-07 S/m was embedded in the domain of a homogeneous electrical conductivity of 0.0034 S/m. The size of the anomaly was

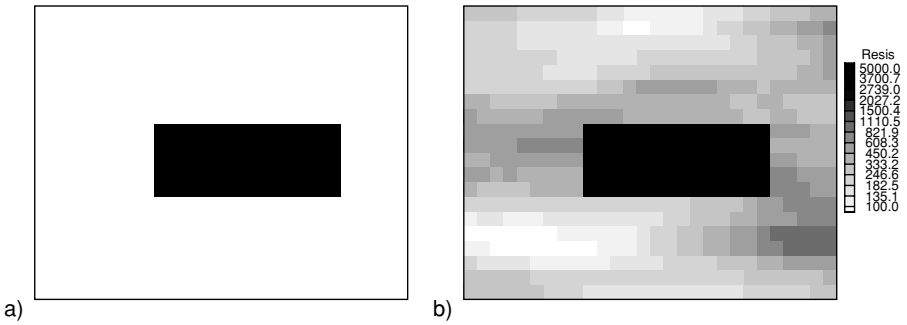

Figure 2. Two synthetic resistivity fields for Example 1: a) A high resistivity rectangle inclusion in a homogeneous resistivity field, and b) a high resistivity rectangle embedded in a random resistivity field

0.14 m by 0.05 m. The left corner of the anomaly was located at (0.09, 0.07) (see Figure 2a); b) instead of embedding it in a homogeneous background electrical conductivity field, the rectangular anomaly was placed in a randomly distributed electrical conductivity field. The mean electrical conductivity of the random field was set to be 0.0034 S/m and the variance of the natural log of the electrical conductivity field was given as 0.3. Its correlation structure was exponential with a correlation of 0.2 m and 0.005 m in the x and y directions, respectively (see Figure 2b). Notice that these electrical conductivity fields of the two scenarios can be considered as nonstationary stochastic fields.

For the two scenarios, ninety six electrodes were placed in each of the elements located around the perimeter of the domain (Figure 3). The ERT survey consisted of 43 transmissions of electric current from a pair of electrodes at different location around the perimeter. During each test, a constant electric current of 0.0001 A was introduced into the domain by one pair of electrodes (transmitting electrodes). The transmitting electrodes were 0.03 m apart. The voltages were then measured in all the 96 electrodes (receiving electrodes). Each voltage measurement was measured from one receiving electrode (a dipole-pole configuration). In total, 43 tests were performed numerically which resulted into 4128 voltage measurements.

Numerical inversions of the transmission current data and voltage measurements were then carried out with the SSLE algorithm. Figures 3 and 4 show the estimated electrical conductivity fields for scenarios a) and b), respectively. As illustrated in these figures, as more current transmissions around the perimeter of the domain are conducted and more pairs of source and resultant voltage field are collected and analyzed, the shape of the anomaly as well as the background conductivity field inside the domain becomes better defined. On the other hand, the rate of the improvement on the estimated

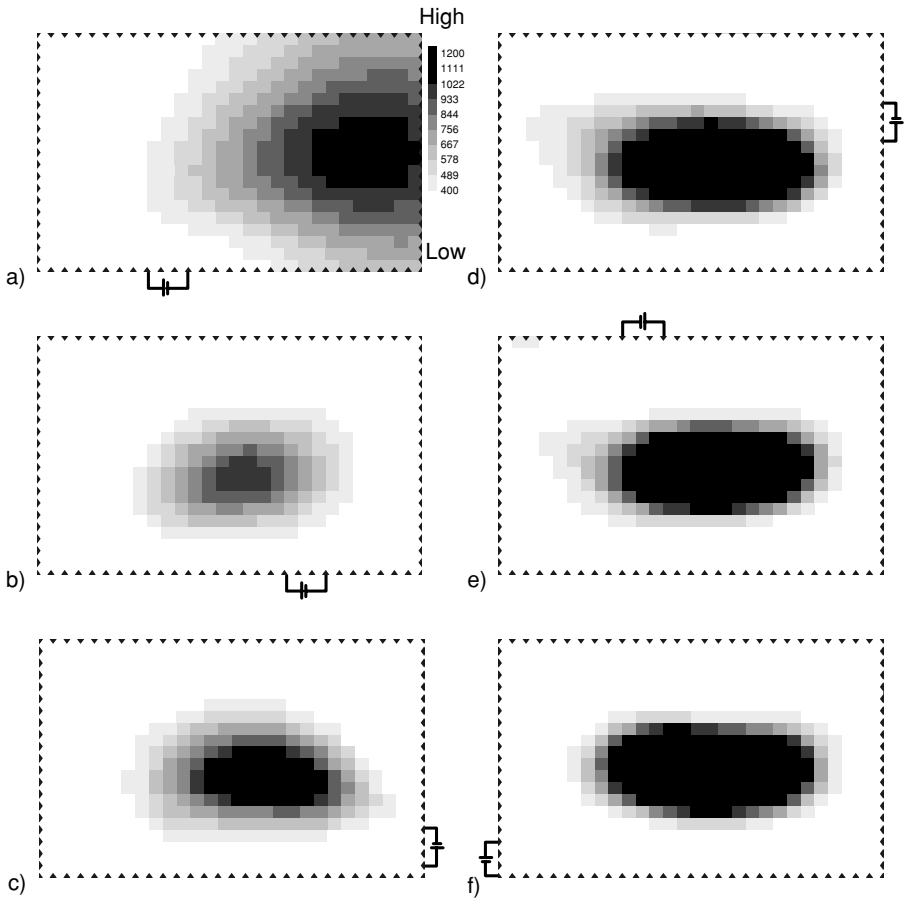

Figure 3. Progression of the estimated resistivity field for case a in example 1 after various numbers of surveys. The battery symbols indicate the location of the source pair

electrical conductivity field diminishes as the number of current transmissions increases.

This example illustrates the intuitive nature of the ERT concept. In essence, ERT is analogous to the human approach inspecting an object: we examine the object from different angles and perspectives – around the perimeter of the object. Light is the source, our eyes are the sensors, and our brain provides the inversion algorithm. Unlike the human brain which provides a "deterministic" rendering of the object, SSLE interprets signals to yield a statistically unbiased image of the object and an uncertainty estimate. This simple example also demonstrates that an inverse problem can be made better posed if sufficient and necessary data are collected. Finally, it should be pointed out

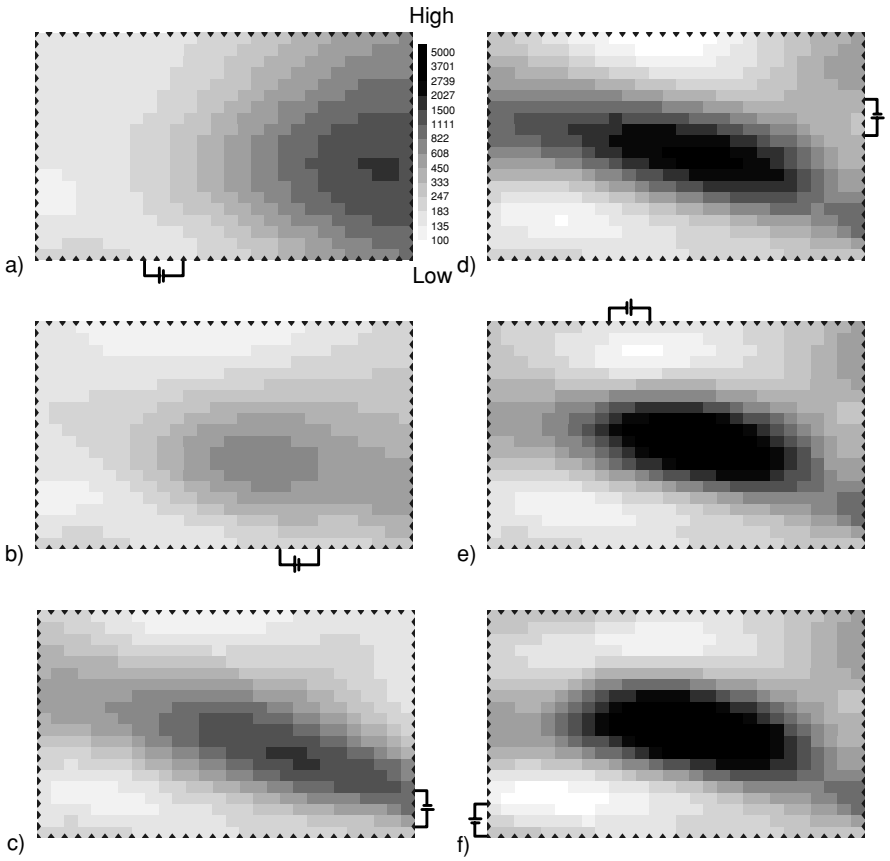

Figure 4. Progression of the estimated resistivity field for case b in example 1 after various numbers of surveys. The battery symbols indicate the location of the source pair

that a tomographic survey is a technique that allows collection of the necessary data set, without invasive probing into the domain.

A similar type of survey called electrical impedance tomography (EIT) has been used as a medical imaging device to "seeing" into human bodies (e.g. Mueller et al., 2002). While the concepts of ERT and EIT are similar, the scales of problems and resolution required in these sciences are significantly different. ERT in subsurface is limited by the number of electric potential sensors and our ability to deploy the sensors to completely surround a geologic medium to be investigated. The variability of electrical resistivity field in geologic media is also more complex and larger in magnitude. Therefore, it is expected that uncertainty in ERT is much greater than that in EIT used in medical sciences.

3.4.2. EXAMPLE 2

Example 2 illustrates the utility of ERT for characterizing migration of contaminants in large-scale geological media. Generally speaking, characterization of transport processes at a field scale based on few local measurements of contaminant concentrations is highly uncertain. Recent field and numerical experiments (e.g. Kemna et al., 2002; Vanderborght et al., 2005) studying transport processes have shown promising results for reducing this uncertainty using ERT. The following synthetic 2D study demonstrates the potential of a joint inversion approach using local concentrations and electrical resistivity measurements for reducing uncertainty and enhancing our ability to characterize and monitor contaminant movements without extensive invasive and costly drilling operations.

In this example, migration of a highly electrically conductive solute plume was simulated in a 2D highly stratified, heterogeneous aquifer with a randomly distributed hydraulic conductivity field. The aquifer was assumed to be free of the solute initially and the aquifer had a uniform electrical conductivity field. A snapshot of the solute plume was then acquired. The concentration distribution of the plume was subsequently converted to a bulk electrical conductivity, σ, distribution based on a linear relation:

$$\sigma = 0.01\ \text{S/m} + c \cdot 0.18\ \text{S/m} \tag{14}$$

where c is the concentration. This conversion led to an electrical conductivity field with a maximum at 0.1 S/m and a background of 0.01 S/m (Figure 5a).

This electrical conductivity field was used to simulate the ERT survey using electrodes located within three boreholes (see Figures 5b or 5c). There were 10 electrodes for each borehole. During the ERT survey a "skip one" dipole-dipole source and measurement array was employed. For each transmission, a current of $+1$ Am or -1 Am is assigned to each electrode of the source pair. The voltage measurements during each current transmission from a source pair were taken at locations starting from one dipole length (1 m) away from the source along the borehole. In the neighboring borehole, the dipole measurements were started from the bottom electrodes, resulting in eight measurements for each borehole. The survey started with the current transmission along the borehole near $y = 5$ m and voltage measurements along the boreholes near $y = 5$ m and 15 m. The source was then moved to the borehole near $y = 15$ m and measurements were taken from the three boreholes. Lastly, the source was moved to the borehole near $y = 25$ m and measurements were taken along the boreholes near $y = 15$ m and 25 m. Altogether this survey consisted of 8 current transmissions at each borehole and 316 dipole-dipole measurements. During the simulation as well as the inversion, no flux boundaries were assumed at the right, left and top of the

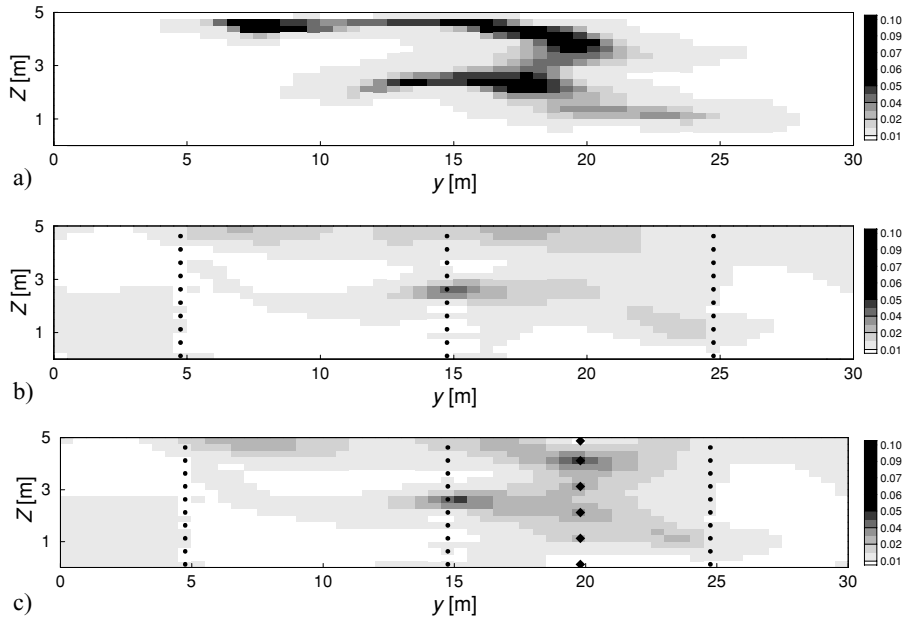

Figure 5. Two dimensional electrical conductivity distributions (S/m): a) synthetically simulated tracer plume, b) inversion results without conditioning, c) inversion results including conditioning. Electrode positions are denoted by dots. Locations of a priori known electrical conductivities are denoted by diamonds

domain. The bottom boundary was set to a constant voltage of 1 V. In an additional borehole the electrical conductivity was assumed to be known a priori at six locations (black diamonds at $y = 20$ m in Figure 5c), representing the result of a borehole resistivity survey.

The SSLE algorithm was subsequently employed to interpret the voltage measurements from the simulated ERT survey. In the first case, the inversion was conducted without point measurements of the resistivity from the six locations along the borehole. Figure 5b depicts the estimated conductivity field for this case. In the second case, the inversion includes the electrical conductivities from the six locations and the resultant conductivity field is shown in Figure 5c. An inspection of Figures 5a–c reveals that the survey captures the general pattern of the electrical conductivity distribution caused by the tracer plume quite satisfactorily. The electrical conductivity anomalies between wells in particular are well represented (Figure 5b) even though no direct concentration measurements are used and the voltage sampling array of the ERT survey is sparse (10 m apart in the horizontal direction) – ERT is indeed a potentially less invasive tool to monitor solute movement in the subsurface. Nonetheless, the estimated electrical conductivity fields are smoother

than those of the true field in Figure 5a. This is attributed to the fact that SSLE seeks a conditional effective parameter field (see Equation 4), which is smooth if insufficient number of conditioning data sets are included. In other words, had more source/voltage measurements been conducted, the estimated field would have been closer to the true field. This finding also supports results of field experiments by Singha and Gorelick (2005).

Figure 5c shows effects of incorporation of the six point electrical conductivity samples from the borehole survey. A comparison of this figure with the other two clearly indicates that inclusion of the point measurements (conditioning using the primary variable) enhances the quality of the inversion results in terms of the pattern and resistivity values significantly. As a result, the example advocates the integration of ERT surveys with direct point measurements.

3.4.3. EXAMPLE 3

The utility of ERT and the SSLE algorithm is demonstrated for monitoring transient water infiltration through 3-D vadose zones in this example. Here, water movement was simulated in a 3-D synthetic vadose zone corresponding to an infiltration event. The vadose zone was assumed to be a cube (2 m on each side) consisting of 2,000 elements in size of 0.2 m $\times$ 0.2 m $\times$ 0.1 m. Random values of the heterogeneous unsaturated hydraulic parameters were generated and assigned to each element using the spectral method (see Liu and Yeh, 2004). The simulated moisture content distribution at 50,000 minutes after the infiltration commenced, $\theta_{50,000}$, (Figure 6a) was used as the true moisture content fields for this demonstration. A power law constitutive relation then related the moisture content to the resistivity (e.g. Yeh et al., 2002):

$$\rho = \rho_0 \theta^{-m} \tag{15}$$

where ρ is bulk electrical resistivity, ρ_0 is a fitting parameter that is related to the electrical resistivity of pore water, m is a dimensionless fitting parameter, and θ denotes volumetric moisture content. We assumed that ρ_0 did not change during the infiltration event.

This constitutive relation (Equation 15) or a similar type of relation has frequently been used by practitioners to translate a resistivity field to a moisture content field as well. In addition, a single constitutive relation is often assumed for a given entire field. Yeh et al. (2002), however, found that the parameters of Equation (15), ρ_0 and m, varied significantly in space under field conditions. They showed that without considering the spatial variability of these parameters, interpretation of moisture content distribution based on Equation (15) can be misleading. In this example, to describe spatial variability in the parameters of the resistivity and moisture content relation in the vadose

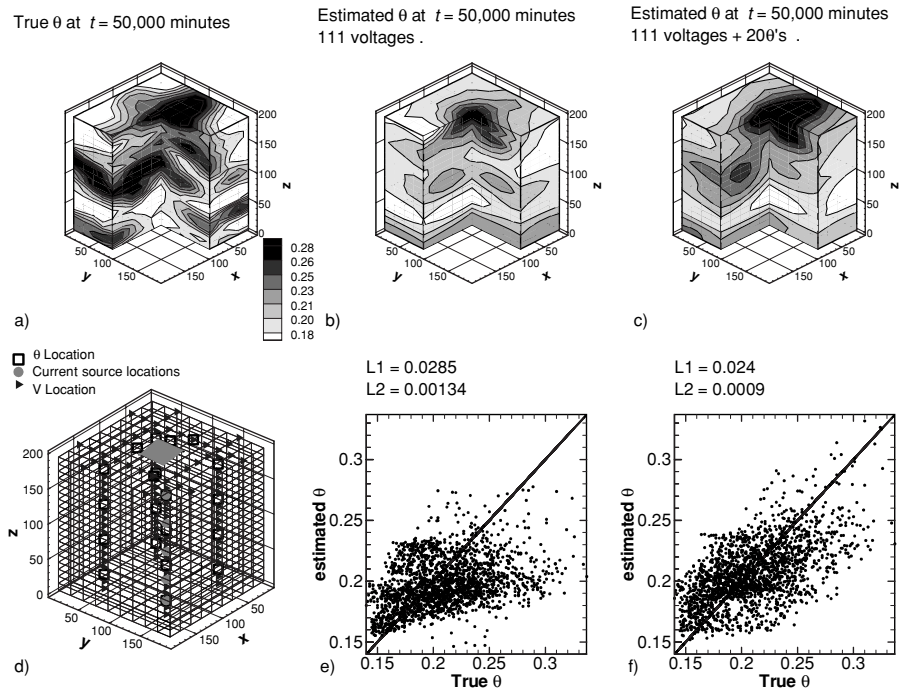

Figure 6. a) true moisture distribution, θ, at time = 50,000 minutes after infiltration; b) estimated moisture content distribution using 111 voltage measurements from the ERT; c) estimated moisture content distribution using the 111 voltage measurements plus 20 direct moisture content measurements; d) the layout for the ERT survey; e) a scatter plot showing the estimated moisture content vs. the true moisture content distribution, corresponding to Figure 6b; f) the scatter plot corresponding to Figure 6c

zone, the two parameters, ρ_0 and m, were considered as random fields with geometric means of 7.036 Ωm and 1.336, respectively. Variances of $\ln\rho_0$ and $\ln m$ were assumed to be 0.633 and 0.034, respectively. We further assumed that both parameters possessed the same exponential correlation structure with a horizontal correlation scale of 0.8 m and a vertical correlation scale of 0.2 m.

Based on these synthetic ρ_0, m and $\theta_{50,000}$ fields, a true resistivity field at 50,000 minutes ($\rho_{50,000}$) after infiltration were calculated using Equation (15). ERT surveys were then simulated using this resistivity field. Figure 6d displays the 3-D layout of the ERT surveys. The design of the ERT survey layout included four boreholes penetrating the entire depth of the simulation domain. The x and y coordinate pairs, in meters, of the four bore holes were (0.5, 0.5), (1.5, 1.5), (0.5, 1.5), and (1.5, 1.5). Each borehole had twenty electrodes. Additional 31 electrodes were deployed along the surface in four lines with endpoints at the above x–y coordinates. Currents were then transmitted

sequentially at the five depths of 0.25, 0.55, 0.95, 1.35, and 1.75 m along the upper right bore hole (1.5, 1.5). The ERT surveys resulted in five current/voltage data sets of 111 voltage measurements each. In addition, we also sampled 20 ρ_0 and m values along each of the four bore holes (a total of 80 measurements). The moisture content θ was sampled at 20 locations indicated by squares in Figure 6d.

To estimate the θ field directly based on the data from the ERT survey, the SSLE algorithm was modified by Liu and Yeh (2004) to include Equation (15), as well as the sample values of ρ_0, m, and θ's. This SSLE is called the integrative SSLE. For the purpose of demonstrating the effect of the direct θ measurements on the estimated moisture content field, we estimated the moisture content distribution at 50,000 minutes for two cases; a) without using any θ measurement and b) with 20 θ measurements in addition to the voltage measurements.

Figures 6a and 6b show the true moisture content distribution at 50,000 minutes and the corresponding estimated moisture content distribution using 111×5 voltage measurements, and 80 pairs of ρ_0 and m measurements, respectively. The estimated field using the same number of voltage, ρ_o and m measurements, but including 20 direct θ measurements, is illustrated in Figure 6c. An inspection of the three figures reveals that the integrative SSLE algorithm reproduces the general pattern of the simulated true moisture content distribution, even though the constitutive relation between resistivity and moisture content varies spatially. Again, the estimated moistue content fields in Figures 6b and 6c are smoother than that in Figure 6a. The inclusion of the 20 θ measurements, on the other hand, greatly improves the estimate of the θ distribution. Figures 6e and 6f are scatter plots that correspond to Figures 6b and 6c, respectively. A 45° line indicates perfect estimation (unbiasedness and zero variance); scattering (variance) around the line is indicative of smoothness of the estimates. According to these two scatter plots, the inclusion of the 20 θ measurements reduces the biasedness of the ERT inversion for moisture content. The goodness of fit was also evaluated using L1 and L2 norms. The reductions in the L1 and L2 norms from Figures 6e to 6f indicate that the addition of moisture content measurements dramatically improve the estimate.

The conditional variance of the estimate from our SSLE approach can be used to assess the uncertainty associated with the estimate: a smaller conditional variance indicates less uncertainty in the estimate. The conditional variances corresponding to the estimates obtained when using zero and 20 θ measurements are shown on Figures 7a and 7b, respectively. Small conditional variances are located closely to the four boreholes where secondary information is measured. At locations where moisture content measurements were collected, the conditional variance is zero, indicating that these observations are honored in the inverse model and that no uncertainty exists.

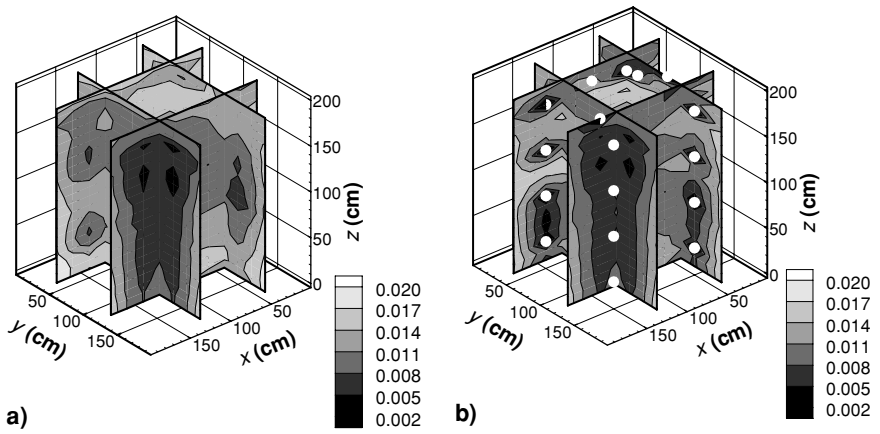

Figure 7. Estimation variance maps corresponding to the estimates in Figures 6b and 6c

3.5. Field Study

Previous numerical examples illustrate the ERT concept and robustness of SSLE. These examples however exclude measurement error and noise. Measurement error and noise are associated to equipment resolution and external electromagnetic sources (natural or induced) and they are inherent in the real-world applications of ERT. In this section we show an application of ERT to monitoring leaching operation in a mine site and demonstrate ways to tackle measurement error and noise, using our stochastic approach.

As a part of the operation of a test module in the Quebrada Blanca (QB) leaching operation in Northern Chile (see Guzman et al., 2006 for a complete description of the experimental setting), an ERT monitoring system was installed early January, 2004. Leaching consists of applying a dilute acid solution on the surface of the heap using a drip irrigation system to promote the removal of metal values. The application rate ranged from 4.2×10^{-4} cm/s to 8.4×10^{-4} cm/s. The duration of the leach cycle is defined as the time at which the desire level of metal extraction (e.g. 80%) is attained. The monitoring system was used to track operational variables (i.e., moisture content, temperature, and oxidation/reduction potential; ORP) for evaluation of the leaching mechanisms within the test module. The system operated during the first half of the leach cycle to 12 June 2004 when the system was dismantled. The monitoring system consisted of 34 probes, emplaced at the site with a horizontal spacing of 1.5 m. Twenty-four probes were installed along the centerline of the eastern cell of the test module with dimensions of 80 m by 40 m by 8 m depth; six along a line perpendicular to the centerline on the center of the cell; and two probes on each of the NW and SE quadrants of the cell.

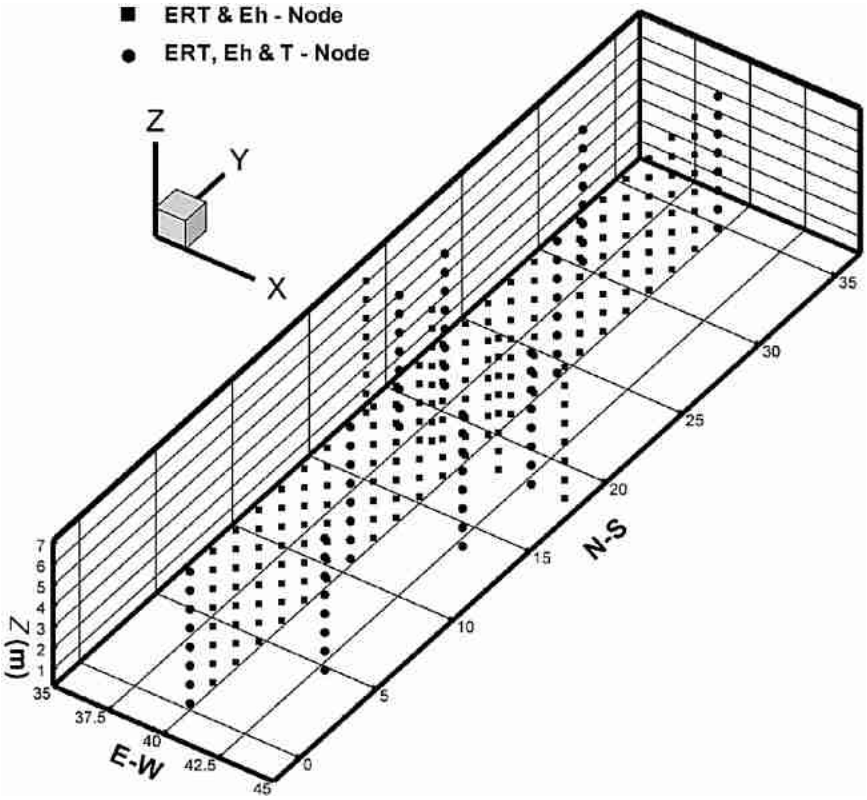

Figure 8. Spatial distribution of ERT electrodes at the QB leaching test module

Each probe was equipped with 8 multi-purpose sensors at a vertical interval of 0.9 m. Figure 8 presents a perspective view of the layout of the monitoring system.

To preprocess the voltage data collected from the ERT survey, a systematic approach similar to the structured groundwater model calibration approach proposed by Yeh and Mock (1996) was used. Specifically, the forward model (Equation 4) is first used to simulate the electric potential field in a homogeneous resistivity field at the site, corresponding to an electric current transmission (one pair of source electrodes). The initial value for the homogeneous electrical resistivity field was obtained based on the rock type of the site. The simulated electric potential field was then considered as the mean electric potential field, $\mu(\mathbf{x})$. This mean field was compared with the measured potential field, constructed by interpolation and extrapolation using the measured electric potential values. This comparison allowed us to diagnose possible systematic errors in the measurements and/or our incorrect estimated mean resistivity field. A scatter plot (Figure 9) of the

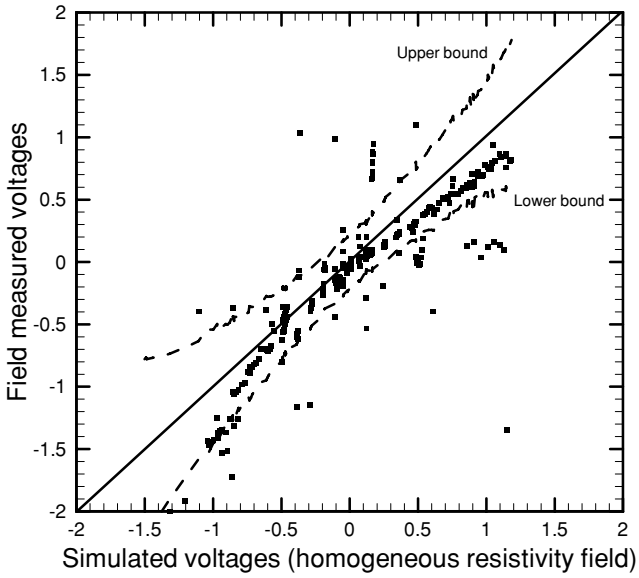

Figure 9. The scatter plot illustrating how the theoretical voltage variance is used to remove noisy measurements

measured values versus the observed ones at all of the measurement locations was also utilized for this purpose. After this diagnostic procedure, measurements of transmissions with systematic errors were eliminated from the following inversion steps. The variance of the electric potential (σ^2) at each measurement location was determined using Equation (11) afterward. The required covariance of the electrical resistivity field in Equation (11) again was specified using prior information. In this example, the prior information was merely an initial guess although the covariance could have been estimated had some borehole resistivity measurements been taken. Notice that the mean and variance calculation process is embedded in the SSLE algorithm.

Next, the estimated standard deviation of the potential value at each measurement location was used to define a low and an upper bound of the electric potential measurements (i.e., $\mu - k\sigma$ and $\mu + k\sigma$, respectively, in which k is an arbitrary integer). Measurements within the upper and the low bound were considered to be statistically reliable given prior knowledge of the spatial variability of the resistivity field at the site. These measurements were selected for the inversion process. Figure 9 illustrates this procedure for a selected transmission of the electric current.

The simulation domain used for the inversion was 34 m in West-East direction, 57 m in North-south direction, and 9.9 m in vertical direction. The domain was discretized into 7106 elements. The corresponding number of

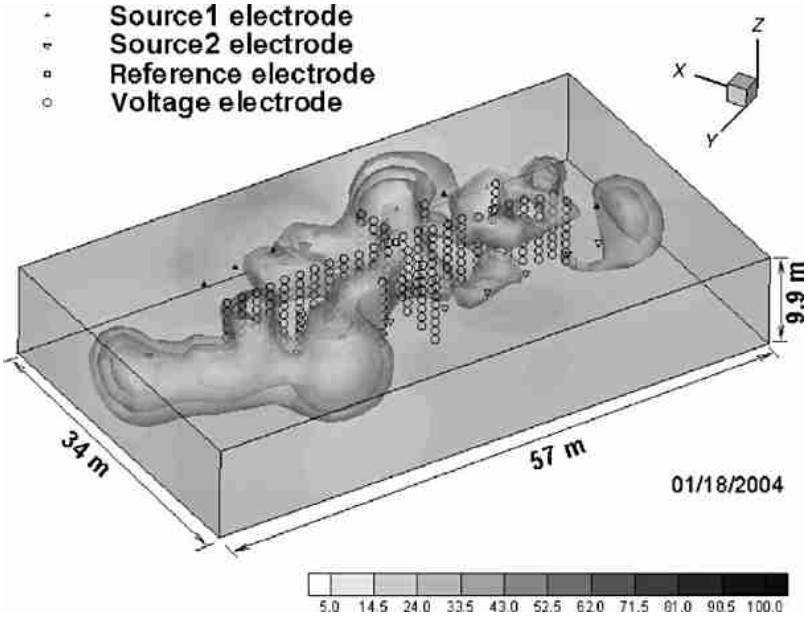

Figure 10a. Estimated resistivity field at the QB site on 18 Jan. 2004

nodes is 8424. The size of each element was 1.5 m (N-S) by 2.0 m (W-E) by 0.9 m (V). The top and bottom surfaces were assumed to be no-flow and the other four sides were considered to be constant voltage boundaries with a value of zero volts. Using the above discretization and boundary conditions, the preprocessed ERT data collected from three different times were analyzed. Figure 10a shows the estimated resistivity field at the site on 18 Jan. 2004. The estimated field for 24 Feb. 2004 is given in Figure 10b and for 22 March, 2004 is in Figure 10c. The total number of measurements used for each inversion was 2700. The computational time for each case was about 4 hours on a cluster consisting of four PCs.

While there were no immediate measurements of in-situ moisture content available to validate our estimated resistivity fields, Figures 10a–c shows increases in volume of low resistivity zones (a general indicator of high moisture content) as the irrigation progressed with time. Measurements of moisture content during the dismantling of the monitoring system showed good correspondence with estimates of moisture content based on the resistivity measurements and lab calibration (Guzman et al., 2006). The evolution of the estimated resistivity fields illustrates the progression of the infiltration process. Moreover, the resistivity measurements delineated the strong correspondence between moisture distribution and surface topography (i.e., zone of high resistivity near the surface correspond to topographic highs while

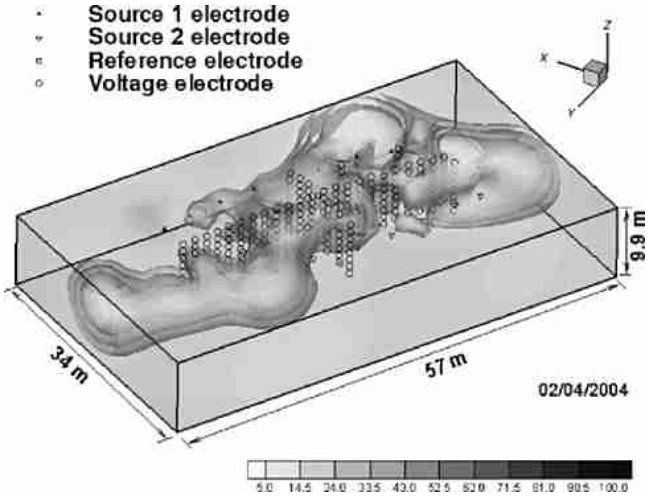

Figure 10b. Estimated resistivity field at the QB site on 24 Feb. 2004

low resistivity areas, wetter zones, correspond to topographic lows). This is quite encouraging since the topographic relief across the surface of the test module is of the order of ± 0.5 m. Other factors and procedures as discussed in Example 3 could have possibly improved the accuracy of our estimates.

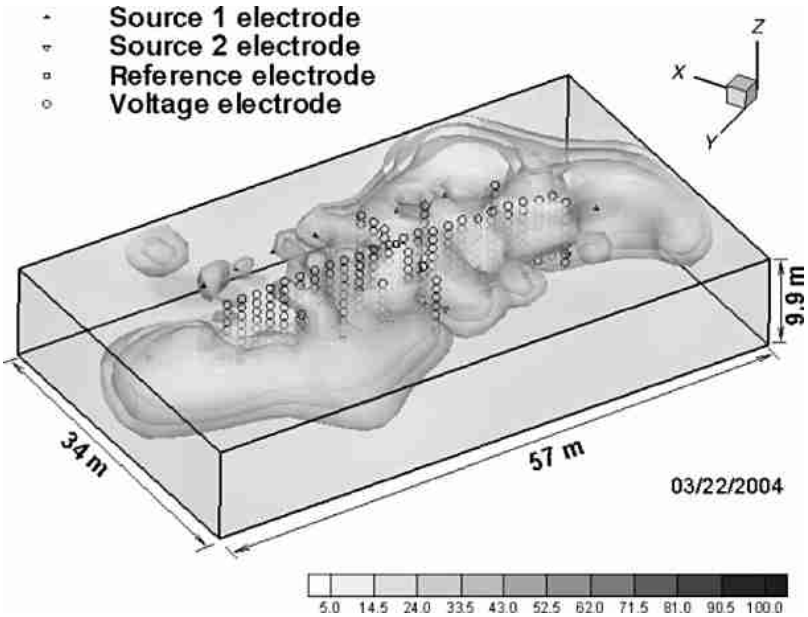

Figure 10c. Estimated resistivity field at the QB site on 22 March 2004

Nevertheless, this field case demonstrates the applicability of our SSLE procedure to a real-world ERT data set.

3.6. Discussions and Conclusion

ERT, instead of the traditional resistivity survey, is an inexpensive and viable technique for the investigation of subsurface resistivity anomalies. It has been listed as one of the most promising near-term science technology targets by a National Technical Working Group of DOE (NTWG, 2004).

Once a resolution of subsurface electrical resistivity anomalies is defined and necessary and sufficient conditions (Yeh and Šimůnek, 2002) are given, a 3-D ERT inversion problem can be well posed at least mathematically. While for most field problems, the necessary and sufficient conditions may be difficult and costly to acquire. A tomographic survey nonetheless offers an intelligent way – common sense – to collect information to make the problem better posed and the estimate as such increases its resolution. For ill- or better-posed problems, a stochastic estimator (such as SSLE) that seeks the condition mean estimate and yields an estimate of its uncertainty is an appropriate choice. Note that stationarity and normality are not required for SSLE to derive good estimates but accurate and dense data sets are. However, the implicit stationarity and normality assumptions do affect the uncertainty derived from SSLE. The uncertainty estimate from any stochastic models, nevertheless, is uncertain itself – statistics is never wrong but can be imprecise. More importantly, the goal of a stochastic estimator is not to predict absolute uncertainty but to provide a quantitative means to assess effectiveness of different sampling strategies.

ERT combined with SSLE or an appropriate stochastic estimator is useful for environmental applications. However, cautions must be taken if an estimated resistivity field is translated to other environmental attributes (such as moisture content, solute concentration, or hydraulic properties of the subsurface). The ambiguity and the spatial variability of the relation between geophysical and other environmental attributes must be considered. For this purpose, an integrative approach (e.g. Liu and Yeh, 2004) or a stochastic information fusion approach (e.g. Yeh and Šimůnek, 2002) is deemed necessary. Likewise, fusion of an ERT survey with a high frequency radar (e.g. ground penetrating radar) survey may enhance our ability to detect subsurface environmental anomalies at higher resolutions and greater depths than either survey by itself.

Lastly, expanding the concept of ERT to basin- or continental-scale electrical resistivity tomographic surveys appears to be logical and feasible although it requires high energy sources. Magnetotellurics (e.g. Vozoff, 1991;

White et al., 2001) in effect is a low frequency, electromagnetic method for continental-scale surveys, which has been used for imaging the electrical conductivity of the Earth. But it does not have the element of the tomographic survey (i.e., examination of the Earth at different angles and perspectives) and its image as such is often equivocal and non-unique. Exploiting cloud-to-ground, direct lightning strikes as a possible energy source (i.e., lightning tomography) for the basin- or continental-scale electromagnetic tomographic surveys as proposed by Yeh (2005) appears to be a logical future research topic in hydrogeophysics.

References

Baker, K., 2001. Investigation of direct and indirect hydraulic property laboratory characterization methods for heterogeneous alluvial deposits: Application to the Sandia-Tech Vadose Zone infiltration test site, Masters Thesis, New Mexico Institute of Mining and Technology, Socorro, NM.

Daily, W., A. Ramirez, D. LaBrecque, and J. Nitao, 1992. Electrical resistivity tomography of vadose water movement, Water Resour. Res., 28 (5), 1429–1442.

Dettinger, M.D., and J.L. Wilson, 1981. First-order analysis of uncertainty in numerical models of groundwater flow, 1, Mathematical development, Water Resour. Res., 17, 149–161.

Ellis, R.G., and S.W. Oldenburg, 1994. The pole-pole 3-D dc resistivity inverse problem: A conjugate gradient approach, Geophys. J. Int., 119, 187–194.

Gavalas, G.R., P.C. Shan, and J.H. Seinfeld, 1976. Reservoir history matching by Bayesian estimation, Soc. Pet. Eng. J., 337–350.

Gelhar, L.W., 1993. Stochastic Subsurface Hydrology, Prentice Hall, Englewood Cliffs, New Jersey.

Gutjahr, A., B. Bullard, S. Hatch, and D.L. Hughson, 1994. Joint conditional simulations and the spectral approach to flow modeling. Stochastic Hydrol. Hydraul., 8 (1), 79–108.

Guzman, A., R.E. Scheffel, and S.M. Flaherty, 2006. Geochemical Profiling of a Sulfide Leaching OperationA Case Study, SME Annual Convention, March 28–31, 2006, St. Louis, MO, USA.

Hanna, S., and T.-C.J. Yeh, 1998. Estimation of co-conditional moments of transmissivity, hydraulic head, and velocity fields, Adv. Water Resour., 22 (1), 87–93.

Hoeksema, R.J., and P.K. Kitanidis, 1984. An application of the geostatistical approach to the inverse problem in two-dimensional groundwater modeling, Water Resour. Res., 20 (7), 1003–1020.

Hughson, D.L., and T.-C.J. Yeh, 2000. An inverse model for three-dimensional flow in variably saturated porous media, Water Resour. Res., 36 (4), 829–839.

Kemna, A., J. Vanderborght, B. Kulessa, and H. Vereecken, 2002. Imaging and characterization of subsurface solute transport using electrical resistivity tomography (ERT) and equivalent transport models, J. Hydrol., 267, 125–146.

Kitanidis, P.K., 1995. Quasi-linear geostatistical theory for inversing, Water Resour. Res., 31 (10), 2411–2519.

Kitanidis, P.K., 1997. Comment on “A reassessment of the groundwater inverse problem” by D. McLaughlin and L.R. Townley, Water Resour. Res., 33(9), 2199–2202.

Kitanidis, P.K., and E.G. Vomvoris, 1983. A geostatistical approach to the inverse problem in groundwater modeling and one-dimensional simulations, Water Resour. Res., 19 (3), 677–690.

Li, B., and T.-C.J. Yeh, 1998. Sensitivity and moment analysis of head in variably saturated regimes, Adv. Water Resour., 21 (6), 477–485.

Li, Y., and D.W. Oldenburg, 1994. Inversion of 3D dc-resistivity data using an approximate inverse mapping, Geophys. J. Int., 116, 527–537.

Li, Y., and D.W. Oldenburg, 2000. Incorporating geological dip information into geophysical inversions, Geophysics, 65 (1), 148–157.

Liu, S., and T.-C.J. Yeh, 2004. An integrative approach for monitoring water movement in the vadose zone, Vadose Zone J., 3, 681–692.

Liu, S., T.-C.J. Yeh, and R. Gardiner, 2002. Effectiveness of hydraulic tomography: Sandbox experiments, Water Resour. Res., 38(4), doi: 10.1029/2001WR000338.

McLaughlin, D., and L. R. Townley, 1996. A reassessment of the groundwater inverse problem, Water Resour. Res., 32 (5), 1131–1161.

Mueller, J.L., S. Siltanen, and D. Isaacson. A direct reconstruction algorithm for electrical impedance tomography. IEEE Trans. Med. Imaging, 21 (6), 555–559.

National Research Council (NRC), 2000. Seeing into the earth: noninvasive characterization of the shallow subsurface for environmental and engineering application, Board on Earth Sciences and Resources, Water Science and Technology Board, Commission on Geosciencce, Environment, and Resources, National Academy Press, Washington, DC.

National Technical Working Group (NTWG), 2004. Natural and passive remediation of chlorinate solvents: Critical evaluation of science and technology targets, WSRC-TR-2003-00328, Westinghouse Savannah River Company, Savannah River Site, Aiken, SC 29808, February 19, 2004.

Oldenburg, D.W., and Y. Li, 1999. Estimating depth of investigation in dc resistivity and Ip surveys, Geophysics, 64 (2), 403–416.

Sharma, Perm V., 1997. Environmental and Engineering Geophysics, Cambridge University Press, Cambridge.

Singha, K., and S. Gorelick, 2005. Saline tracer visualized with three-dimensional electrical resistivity tomography: Field-scale spatial moment analysis. Water Resour. Res., 41, W05023, doi: 10.1029/2004WR003460.

Sun, N.Z., 1994. Inverse Problems in Groundwater Modeling, Kluwer Academic Press, Norwell, MA.

Sun, N.-Z., and W.W.-G. Yeh, 1992. A stochastic inverse solution for transient groundwater flow: Parameter identification and reliability analysis, Water Resour. Res., 28 (12), 3269–3280.

Sykes, J.F., J.L. Wilson, and R.W. Anderews, 1985. Sensitivity analysis for steady state groundwater flow using adjoint operators, Water Resour. Res., 21 (3), 359–371.

Theis, C.V., 1935. The relation between lowering the piezometric surface and the rate and duration of discharge of a well using ground water storage, in 16th Annual Meeting of the Transactions of the American Geophysical Union, Part 2, 519–524.

Tikhonov, A.N., and V.A. Arsenin, 1977. Solutions of Ill-posed Problems. Winston, Washington.

Vanderborght, J., A. Kemna, H. Hardelauf, and H. Vereecken, 2005. Potential of electrical resistivity tomography to infer aquifer transport characteristics from tracer studies: A synthetic case study, Water Resour. Res., 41, W06013, doi: 10.1029/2004WR003774.

Vargas-Guzman, J.A., and T.-C.J. Yeh, 1999. Sequential kriging and cokrging: Two powerful geostatistical approaches, Stochastic Environ. Res. Risk Assess., 13, 416–435.

Vargas-Guzmán, J.A., and T.-C.J. Yeh, 2002. The successive linear estimator: A revisit, Adv. Water Resour., 25, 773–781.

Vozoff, K., 1991. The magnetotelluric method, in Electromagnetic Methods in Applied Geophysics – Applications, Chapter 8, edited by M.N. Nabighia, Society of Exploration Geophysicists.

White, B.S., W.E. Kohler, and L.J. Srnka, 2001. Random scattering in magnetotellurics, Geophysics, 1, 188–204.

Wu, C.-M., T.-C.J. Yeh, J. Zhu, T.H. Lee, N.-S. Hsu, C.-H. Chen, and A.F. Sancho, 2005. Traditional analysis of aquifer tests: Comparing apples to oranges?, Water Resour. Res., 41, W09402, doi: 10.1029/2004WR003717.

Yeh, T.-C.J., 1992. Stochastic modeling of groundwater flow and solute transport in aquifers, J. Hydrol. Process., 6, 369–395.

Yeh, T.-C.J., 1998. Scale issues of heterogeneity in vadose-zone hydrology, in Scale Dependence and Scale Invariance in Hydrology, edited by G. Sposito, Cambridge Press, Cambridge, MA.

Yeh, T.-C.J., 2005. Exploiting natural recurrent stimuli for "seeing" into groundwater basins, in Fall AGU Meeting, SF.

Yeh, T.-C. J., A.L. Gutjahr, and M. Jin, 1995. An iterative cokriging-like technique for groundwater flow modeling, Groundwater, 33 (1), 33–41.

Yeh, T.-C.J., and J. Šimůnek, 2002. Stochastic fusion of information for characterizing and monitoring the vadose zone, Vadose Zone J., 1, 207–221.

Yeh, T.-C.J., M. Jin, and S. Hanna, 1996. An iterative stochastic inverse method: Conditional effective transmissivity and hydraulic head fields, Water Resour. Res., 32 (1), 85–92.

Yeh, T.-C.J., and S.Y. Liu, 2000. Hydraulic tomography: Development of a new aquifer test method, Water Resour. Res., 36 (8), 2095–2105.

Yeh, T.-C.J., S. Liu, R. J. Glass, K. Baker, J. R. Brainard, D. Alumbaugh, and D. LaBrecque, 2002. A geostatistically based inverse model for electrical resistivity surveys and its applications to vadose zone hydrology, Water Resour. Res., 38 (12), 1278, doi: 10.1029/2001WR001024.

Yeh, T.-C.J., and P.A. Mock, 1996. A structured approach for calibrating steady-state ground water flow models, Groundwater, 34 (3), 444–450.

Yeh, T.-C.J., and J. Zhang, 1996. A geostatistical inverse method for variably saturated flow in vadose zone, Water Resour. Res., 32 (9), 2757–2766.

Yeh, W.W.-G., 1986. Review of parameter identification procedures in groundwater hydrology: The inverse problem, Water Resour. Res., 22 (1), 95–108.

Zhang, J., and T.-C.J. Yeh, 1997. An iterative geostatistical inverse method for steady flow in the vadose zone, Water Resour. Res., 33 (1), 63–71.

Zhang, J., R.L. Mackie, and T. Madden, 1995. 3-D resistivity forward modeling and inversion using conjugate gradients, Geophysics, 60, 1313–1325.

Zhu, J., and T.-C.J. Yeh, 2005. Characterization of aquifer heterogeneity using transient hydraulic tomography, Water Resour. Res., 41, W07028, doi: 10.1029/2004WR003790.